# Supporting Information

**Large-scale semi-embedded AgNWs-based stretchable transparent electrodes via superwettability-induced transfer of AgNWs/ionic liquid onto gradient PDMS**

Shoujie Shen,*[a] Qiyu Wu,[a] Xingchao Chen,[b] Jia Li,[a] Xuanting Zhao,[b] Chuao Ma,[b] Chan Liu[b] and Hongliang Liu*[b,c]

[a.]Key Laboratory of Magnetic Molecules and Magnetic Information Materials (Ministry of Education), School of Chemistry and Material Science, Shanxi Normal University, Taiyuan 030031, P. R. China

[b.]School of Chemistry and Chemical Engineering Yantai University, Yantai 264006, P. R. China

[c.]Shandong Laboratory of Advanced Materials and Green Manufacturing at Yantai, Yantai, 264006, P. R. China

E-mail: shoujie_shen@outlook.com; liuhongliang@ytu.edu.cn

## 1. Fabrication of gradient PDMS

Fig. S1a shows the process of platinum-catalyzed polymerization between a dimethylsiloxane oligomer with vinyl terminal groups and a curing agent (dimethyl methylhydrogen siloxane) containing a –Si-H bond using hydrosilylation reaction.[1] It involves the catalytic addition of Si-H groups to a C=C double bond to form the Si-C bonds. The crosslinking density of PDMS can be tuned by varing curing time. As shown in Fig. S1b, the peak intensity at 2150 $cm^{-1}$ ascribing to –Si-H decreases gradually with increasing curing time by using the peak at 1300 $cm^{-1}$ ascribing to –Si-$CH_3$ as reference, indicating increased crosslinking density with increasing curing time. The generated gradient PDMS exhibits distinct mechanical strength. The bottom PDMS cured for 1 h is tougher with higher modulus of 0.35 kPa than the top PDMS cured for 8 min with lower modulus of 0.03 kPa (Fig. S1c). We further use nanoindentation to evaluate the mechanical property of the gradient PDMS. As shown in Fig. S1e, six points are collected at intervals of 40 μm from top to bottom, and moduli of the sample increase from point 2 to point 5, owing to the increased crosslinked density. The thickness of the gradient region (from point 2 to point 5) is about 120 μm.

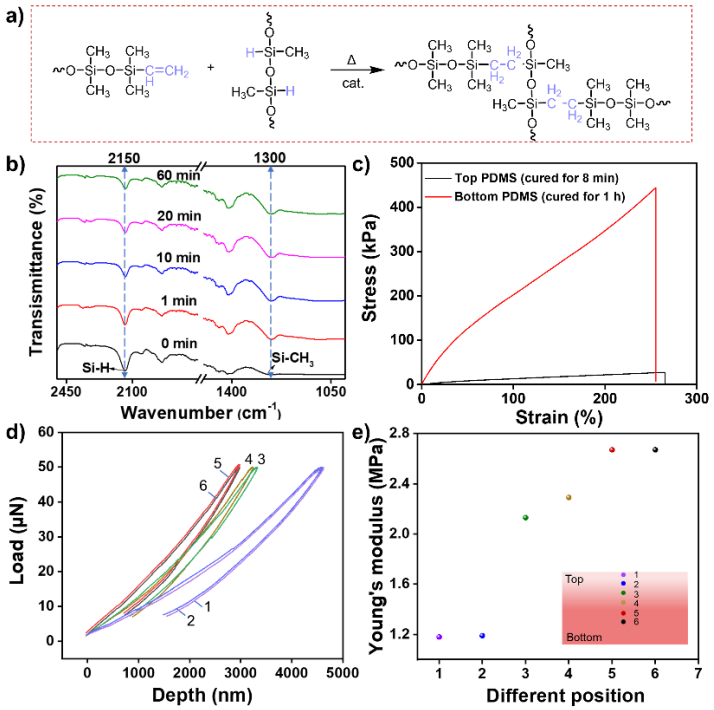


**Fig. S1** a) Scheme showing crosslinking mechanism of PDMS. b) FTIR spectra of PDMS with different curing time. c) Stress-strain curves of PDMS cured for 8 min and

1 h, respectively. d) Nanoindentation load-depth curves obtained for gradient PDMS samples. e) Evolution of the Young's modulus at different positions.

**2. Pretreatment of the PDMS substrates before superwettability-transfer**

The original gradient PDMS is hydrophobic with water contact angle (WCA) of 123 (Fig. S2a). After plasma-treatment at a power of 40 W for 50 s, the PDMS becomes superhydrophilic (Fig. S2b), which is essential for the subsequent transfer of AgNWs/[EMIm]$NTf_2$ complex.

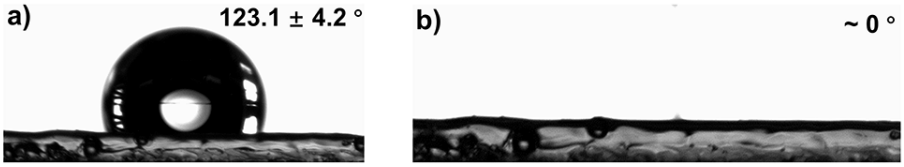


**Fig. S2** As-prepared hydrophobic PDMS with WCA of 123.1 ± 4.2° (a) becomes superhydrophilic with WCA of 0° after plasma treatment (b).

**3. Improve the conductivity of the STEs by electro-less welding**

After transferring the AgNWs/[EMIm]$NTf_2$ complex onto the gradient PDMS, the STEs were released and further electroless-welded according to our previous reports. Specifically, the STE was dipped into a mixed solution of silver-ammonia and glucose (0.5%) with ratio 1:1 for several minutes to improve the conductivity of the STE. The silver-ammonia solution was first prepared by mixing 10 mL silver nitrate solution (0.2%), 1 mL sodium hydroxide solution (1%), and 6 mL aqueous ammonia solution (0.2%). Then, the STE was rinsed with distilled water and vacuum drying at 60 $^{o}$C for 1 h. Here, the welding time is an important parameter for the STEs to achieve better optoelectrical properties. On one hand, increasing welding time can greatly reduce the contact resistance of the AgNWs. On the other hand, however, increasing welding time would generate silver nanoparticles on the PDMS substrates, thus reducing the optical transmittance of the STEs. Considering both sheet resistance and optical transmittance of the STEs, welding time of 15 s is chosen as the optimal condition (Fig. S3).

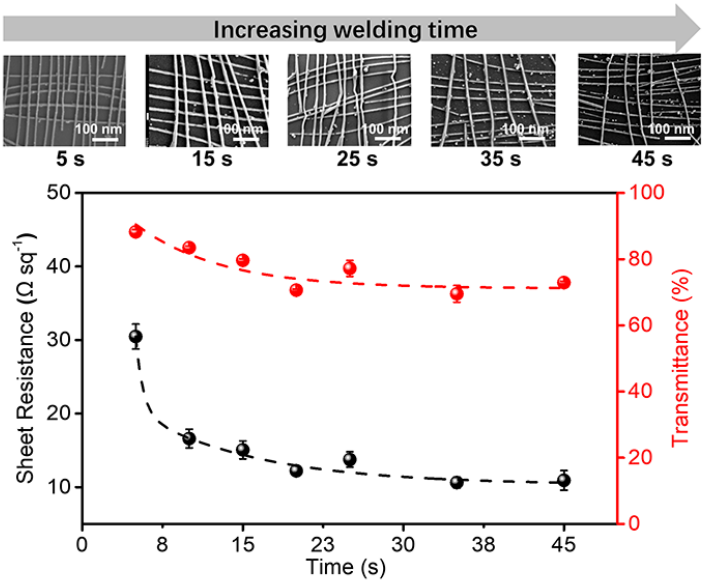


**Fig. S3** The variation diagram of sheet resistance and optical transmittance of STEs with welding time.

**4. Mechanical stability of the STEs**

The gradient PDMS with low cross-linked interfacial layer can result in semi-embedding of AgNWs into the PDMS, thus providing improved adhesion between AgNWs and PDMS. As shown in Fig. S4, after repeated treating the STEs with 3M adhesive tape for 15 cycles, $\Delta R/R_0$ for WG/WPT is only 3.4, while that for WOG/WPT is 27.2. Even worse, $\Delta R/R_0$ for WOG/WOPT reaches 320 after 5 cycles. Therefore, gradient PDMS can endow the STE with improved mechanical stability. We also compared the sheet resistance, optical transmittance and mechanical stretchability of our designed WG/WPT with reported STEs (Fig. S5).

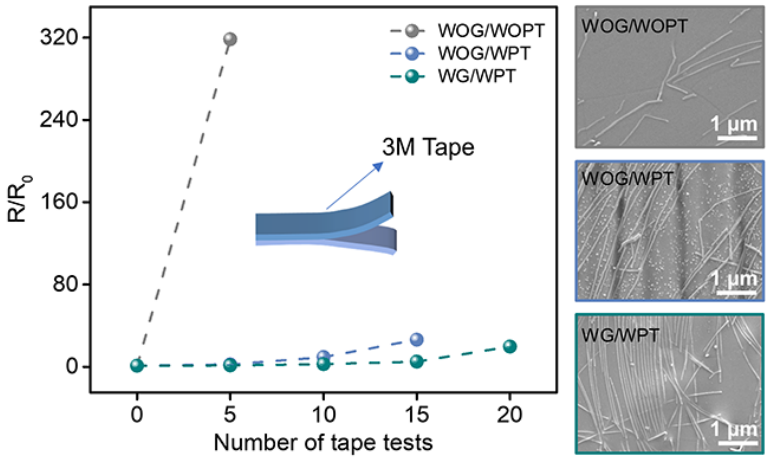


**Fig. S4** Variation of $\Delta R/R_0$ with number of tape tests for WOG/WOPT, WOG/WPT and WG/WPT. Insets: The SEM images of WOG/WOPT, WOG/WPT and WG/WPT after being taped for 15 times.

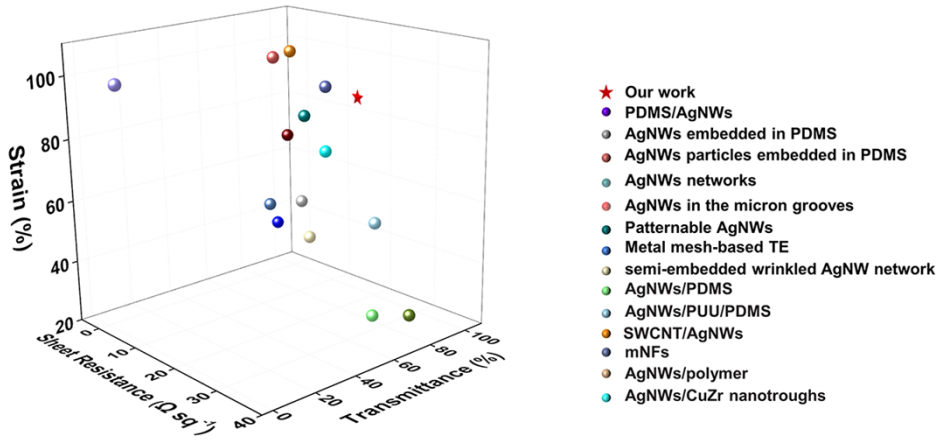


**Fig. S5** Comparison of the optoelectronic performance and stretchability of the as-reported STEs such as PDMS/AgNWs,[2] AgNWs embedded in PDMS,[3] AgNWs particles embedded in PDMS,[4] AgNWs networks,[5] AgNWs in the micron grooves,[6] patternable AgNWs,[7] metal mesh-based TE,[8] AgNWs/PDMS,[9,10] AgNWs/PUU/PDMS,[11] SWCNT/AgNWs,[12] mNFs,[13] AgNWs/polymer[14] and AgNWs/CuZr nanotroughs.[15] Our designed STEs exhibit comparable optoelectronic performance and relatively high stretchability.

## 5. Thermal stability of the electro-heating devices

The thermal stability of the electro-heating device prepared by using WG/WPT with sheet resistance of 15 Ω $sq^{-1}$ was examined. DC voltage was applied between two sides of the STE, while the voltage was increased by 1 V every 10 min. The temperature variation with time curves by placing the WG/WPT STE samples at platform voltages of 4, 5, 6 and 7 V for ten minutes each through voltage platform experiments (Fig. S6).

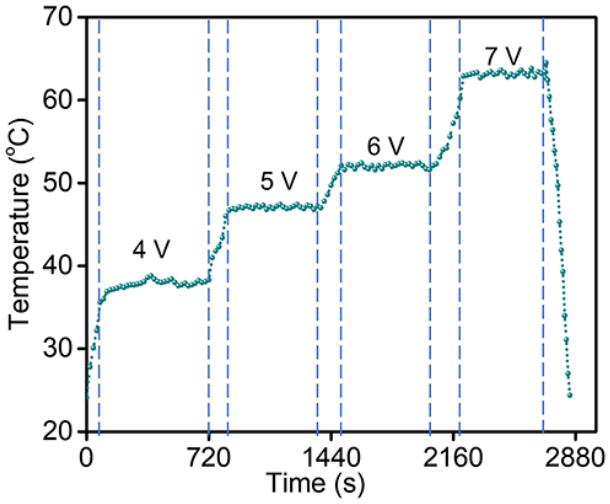


**Fig. S6** Steady-state temperature of the STE record during voltage plateau experiments.

## 6. The microstructure of the EL device

The EL device was constructed with a sandwiched structure, where a light-emitting layer (ZnS:Cu/PDMS) was inserted between a pair of WG/WPT. The thinkness of the light-emitting layer is about 172 μm.

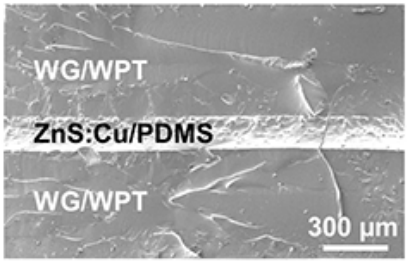


**Fig. S7** The side view of the EL device.

## References


1 S. Li, J. Zhang, J. He, W. Liu, Y. Wang, Z. Huang, H. Pang, Y. Chen, *Adv. Sci.*, 2023, **10**, 2304506.

2 Y. Feng, J. Song, G. Han, B. Zhou, C. Liu, C. Shen, *Small Methods*, 2023, **7**, 2201490.

3 P. Zhang, X. Tong, Y. Gao, Z. Qian, R. Ren, C. Bian, J. Wang, G. Cai, *Adv. Funct. Mater*., 2023, **33**, 2303270.

4 S. Zhang, Y. Li, Q. Tian, L. Liu, W. Yao, C. Chi, P. Zeng, N. Zhang, W. Wu, *J. Mater. Chem. C*, 2018, **6**, 3999-4006.

5 S. Cho, S. Kang, A. Pandya, R. Shanker, Z. Khan, Y. Lee, J. Park, S.L. Craig, H. Ko, *ACS Nano.*, 2017, **11**, 4346-4357.

6 T. Hao, L. Zhang, H. Ji, Q. Zhou, T. Feng, S. Song, B. Wang, D. Liu, Z. Ren, W. Liu, Y. Zhang, J. Sun, Y. Li, *Polymers*, 2023, **15**, 2640.

7 Y. Gu, Z. Qiu, S. Zhu, H. Lu, L. Peng, G. Zhang, Z. Wu, X. Gui, Z. Qin, B.-r. Yang, *Nano Res*., 2023, **16**, 11303-11311.

8 H. Hu, S. Wang, S. Wang, G. Liu, T. Cao, Y. Long, *Adv. Funct. Mater*., 2019, **29**, 1902922.

9 H. Fan, K. Li, Q. Li, C. Hou, Q. Zhang, Y. Li, W. Jin, H. Wang, *J. Mater. Chem. C*, 2017, **5**, 9778-9785.

10 X. Chen, Y. Zhang, C. Ma, H. Liu, *Chem. Eng. J*., 2023, **476**, 146505.

11 D.-H. Kim, K.-C. Yu, Y. Kim, J.-W. Kim, *ACS Appl. Mater. Interfaces*, 2015, **7**, 15214-15222.

12 B.-Y. Hwang, S.-H. Choi, K.-W. Lee, J.-Y. Kim, *Compos. Part B Eng*., 2018, **151**, 1-7.

13 J. Jang, B.G. Hyun, S. Ji, E. Cho, B.W. An, W.H. Cheong, J.-U. Park, *NPG Asia Mater*., 2017, **9**, e432.

14 Y. Chen, R.S. Carmichael, T.B. Carmichael, *ACS Appl. Mater. Interfaces*, 2019, **11**, 31210-31219.

15 S. Lee, S.-W. Kim, M. Ghidelli, H.S. An, J. Jang, A.L. Bassi, S.-Y. Lee, J.-U. Park, *Nano Lett*., 2020, **20**, 4872-4881.